Kütahya Dumlupınar University
Institute of Graduate Studies

Journal of Scientific
Reports-A
E-ISSN: 2687-6167
Number 47, June 2021

RESEARCH ARTICLE

HYDROGEN PRODUCTION from HYDRAZINE on SOME TRANSITION METAL (Sc, Ti and V) -EMBEDDED GRAPHENE

Hilal Küçük[1]

Gazi University, Department of Physics, Ankara, hilakucuk@gazi.edu.tr, ORCID: 0000-0002-0777-1102

Received Date:18.05.2021 *Accepted Date:06.10.2021*

ABSTRACT

The investigation of N2H4 decomposition catalysts is a highly popular subject because of the demand for clean and renewable energy sources. Herein, N_2H_4 adsorption energy and decomposition kinetics are analyzed to find a better 2D single-atom catalyst (SAC) using modified graphene by embedding light 3d-transition metals. Hydrogen selection of hydrazine decomposition over Sc,Ti and V atoms catalysts are studied on two pathways: the N-N bond scission ($N_2H_4 \rightarrow NH_2 + NH_2$) and N-H bond split ($N_2H_4 \rightarrow N_2H_3 + H$). On graphene embedded by Sc and Ti metal produces easily $2NH_2$ because their activation energy is almost close to 0 eV. The activation of energy of N-H cleavage on graphene embedded by vanadium atom is lower (0.99 eV) than that of N-N cleavage (1.36 eV). Therefore, H production from hydrazine on V metal surface is more favorable than $2NH_2$ production.

Keywords: *TM embedded graphene with single vacancy; hydrazine decomposition; hydrogen generation; single-atom catalysis.*

1. INTRODUCTION

After industrial growth, enormous energy in the order of exajoules is needed because of the increment of the human population, and this demand is increasing more and more each day[1]. Conventional energy is produced by natural coal, gas, oil and nuclear energy, coal, oil, wood, and coal. However, they cause serious global warming and traditional fuels are not renewable. Nowadays, industrial countries endeavor to investigate completely carbon-free and sustainable economies within the next decades[1-3]. For reaching carbon-free energy sources, hydrazine (N_2H_4) can be exploited through the high hydrogen continent of hydrazine (12.5 wt %) as a mobile hydrogen source[4-6]. N_2, H_2, and $NH_3$with hydrogen (H) can be generated through its decomposition without harmful carbon productions[7]. The application areas of hydrazine are fuel cells as a portable battery in space ships, automobiles, and laptops, agriculture for the preparation of pesticides, and the missile system for the military [8, 9]. Hydrazine can appear as gauche, cis and anti due to the internal rotation of NH_2 group around N-N bond [10-13]. The large dipole moment

of gauche conformation and the coplanar repulsions in the cis and anti-conformation cause that hydrazine tends to appear as gauge form in the gas phase [14, 15].

There are many researches to understand catalysts effects on hydrazine such as, bare surface; Ni (111), Ir(111) [16], Pt(111) [11], Ni (111)[17], Fe(211) [18], Cu(111)[19], monometallic nanoparticle catalysts[5]. Due to increase catalytic effects, transition metal alloys are used as well. For instance, $Ni_xM_8/Ni(111)$ (M is transition metal, x=8,14,15) materials are investigated for adsorption of hydrazine. The finding is that these surfaces are much more effective candidates than Ni(1 1 1) sheet for hydrazine adsorption [20].

N-N bond can be broken more easily because N-N bond is weaker than N-H bond in gaseous. Therefore, an effective catalyst for dehydrogenation from hydrazine has not yet been found until now[21]. However, research on hydrogen production from hydrazine is crucial and still needed because of clean energy using hydrogen. The investigations on graphene embedded by transition metal are necessary for many reactions because they can be one of the effective, durable, and affordable catalysts[22, 23]. Transition-metal-carbon materials can be inexpensive compared to metal-based catalysts. In this study, graphene is modified by embedding with some light 3d transition metal to change its magnetic properties and bandgap. Our goal is to achieve a better catalytic effect on hydrazine decomposition. For hydrogen generation, N-H bond cleavage will be worked compared with N-N bond cleavage on graphene embedded surfaces.

2. COMPUTATIONAL DETAIL

Using density functional theory (DFT), all analyses were calculated with Quantum Espresso software package[24, 25]. (PAW) potential (pbe-n-kjpaw) were chosen[26, 27]. The kinetic energy parameter for wavefunctions was 50 Ry for Sc and V metal, and 55 Ry for Ti metal. This energy parameter for potential and charge density was 500 Ry for Ti metal and V metal, and 402 Ry for Sc. Three surfaces were modeled with 4x4x1 cells and 32 atoms. To contain van der Waals interactions corrections the term Grimme-D2 was implemented[28]. The lattice parameters are a=9.8 Å and c=20 Å and also Monkhorst-Pack k-point grid is 4x4x1.

The central M transition metals (Sc, Ti, V) are embedded in the graphene sheet. The surface models with different perspectives are seen in Figure 1.

JSR A
Journal of Scientific Reports

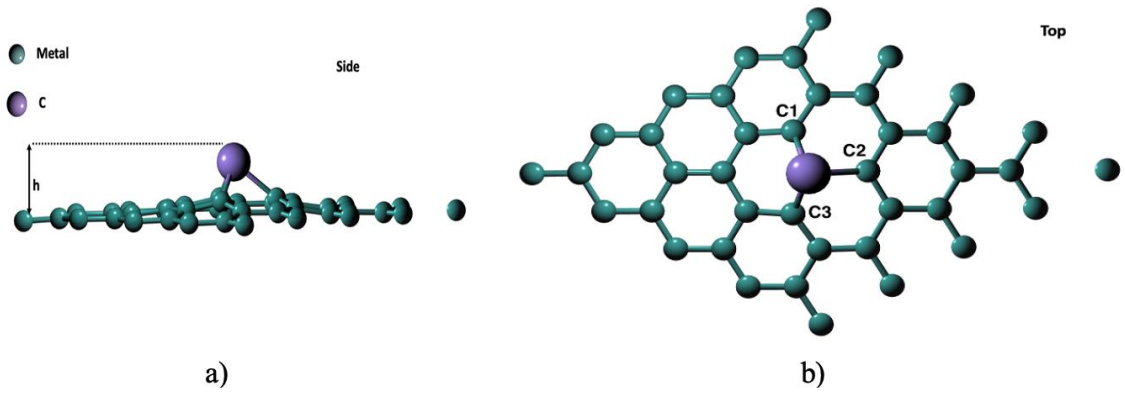

Figure 1. M (Sc, Ti and V) embedded into graphene surface a) Graphene sheet from side view b) Graphene sheet from the top view. The colors of C and transition metal are green and violet respectively.

Table 1 represents the distance between the transition metal and C atom on the lowest level, bond distances, magnetic moments after optimization for the different surfaces. In all sections, the result will be given in order such as Sc, Ti, and V metal, unless stated otherwise. According to the previous research by G. Santos's group[29], the heights are ~1.7 Å, ~1.5 Å, ~1.4 Å and the bond distances between metal and C atoms ($\boldsymbol{d_{M-C}}$) are ~2.1 Å, ~1.95 Å, ~1.85 Å. Additionally, the magnetics are 0.0 μ_B, 0.0 μ_B, 1.0 μ_B. The finding between mentioned study and our findings in Table 1 are quite close to each other.

Table 1. The bond distances, magnetic moments after optimization for the different surfaces.

M	Distance-h (Å)	$\boldsymbol{d_{M-C_1}}$, $\boldsymbol{d_{M-C_2}}$, $\boldsymbol{d_{M-C_3}}$ (Å)	Magnetic Mom. (μ_B)
Sc	1.7	2.06	0.0
Ti	1.5	1.92	0.0
V	1.4	1.88	1.0

The adsorption energies (E_{ads});

$$E_{ads} = E_{\text{M- graphene+molecule}} - E_{\text{M- graphene}} - E_{\text{molecule}} \quad (1)$$

While the total energy of the adsorption system and the total energy of the surface are respectively $E_{\text{M-graphene+molecule}}$ and $E_{\text{M-N4 in graphene}}$ and, also E_{molecule} is the energy of molecule in the gas phase. A negative E_{ads} value shows a release of energy during adsorption.

JSR A
Journal of Scientific Reports

NEB method (the nudged elastic band) determines the transition state (TS) for reactions [30, 31]. The activation (E_{act}) is

$$E_{act} = E_{TS} - E_{IS} \quad (2)$$

The reaction energy (E_r) is,

$$E_R = E_{FS} - E_{IS} \quad (3)$$

The process is exothermic if $E_R$is negative. Its positive sign is endothermic. E_{TS} is the energy of Transition State, and $E_{IS/FS}$ is the energy of the initial state (IS) or the final state (FS).

3. RESULT AND DISCUSSION

3.1 Adsorption of N_2H_4 and NH_2 in graphene-embedded by M = Sc, Ti and V surface

Gauche conformer of hydrazine was observed on the lowest energy structure on graphene embedded surfaces although it has three different formations known as gauche, trans, and eclipsed in nature. Figure 2 illustrates the molecule on graphene embedded surfaces after optimization. After optimization, while almost all bond lengths of N-H increase, the bond lengths of $N_2 - H_3$ remain the same on Ti and V metal surfaces as seen in Table 2. There are increments on N-N bonds of adsorbed hydrazine, 1.455 $\dot{A}$ for Sc, 1.457 $\dot{A}$ for Ti, 1.456 $\dot{A}$ for V metal from 1.44 $\dot{A}$ on gas phase. The bonds M-N are 2.47 $\dot{A}$ for Sc metal, 2.33 $\dot{A}$ and 2.23$\dot{A}$ for Ti and V metal.

The highest adsorption energy belongs to V embedded surface, -1.49 eV, others are-1.31 eV for Ti metal and -1.22 eV for Sc metal. If the distance between the molecule and the surface is smaller, the adsorption energy is much higher because high interaction occurs between hydrazine and the surfaces. According to the bond lengths and the adsorption energies, the interaction on all surfaces is chemical. These adsorption energy values are higher than that of Li-decorated graphene sheets worked by H. Zeng and colleagues (-1.004 eV) [32].

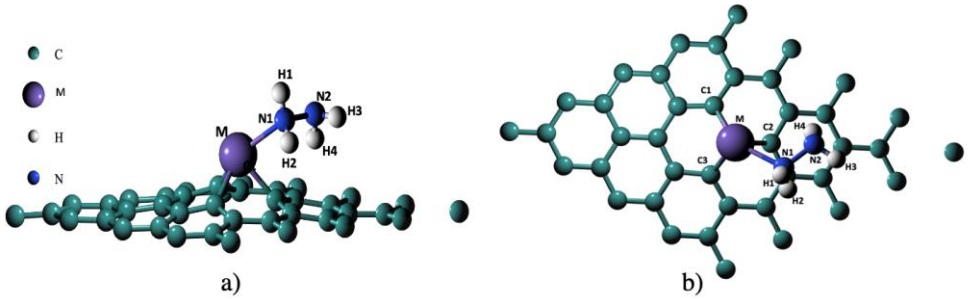

Figure 2. Hydrazine molecule on graphene surface embedded M (M=Sc, Ti, V) a) Side view b) Top view. C atom, M metal, N atom and H atom are illustrated by green, violet, blue and white colors respectively.

JSR A
Journal of Scientific Reports

Δq is known as the electron transfer found by subtracting the charge in adsorbed hydrazine on the graphene embedded sheet from the charge in the gas phase using Bader charge analysis[33]. The meaning of the negative sign of Δq is donating electron while the positive sign is gaining electron from the molecule. Hydrazine molecule gains the most electrons (0.038 e^-) on V metal surface which has the highest adsorption energy. If Table 2 is considered, the adsorption energy has a relationship with the charge transfer. Higher adsorption energy is higher than the charge transfer.

Table 2. Related parameters for N_2H_4 on M embedded graphene.

	E_{ads} (eV)	d_{M-N_1} $(\dot{A})$	$d_{N_1-N_2}$ $(\dot{A})$	$d_{N_1-H_1}$ $(\dot{A})$	$d_{N_1-H_2}$ $(\dot{A})$	$d_{N_2-H_3}$ $(\dot{A})$	$d_{N_2-H_4}$ $(\dot{A})$	$\Delta q(N_2H_4)$ (e^-)
N_2H_4 in gas phase			1.44	1.021	1.025	1.025	1.021	
Sc	-1.22	2.44	1.455	1.023	1.032	1.026	1.028	0.015
Ti	-1.31	2.33	1.457	1.023	1.031	1.025	1.027	0.032
V	-1.49	2.23	1.456	1.024	1.031	1.25	1.028	0.038

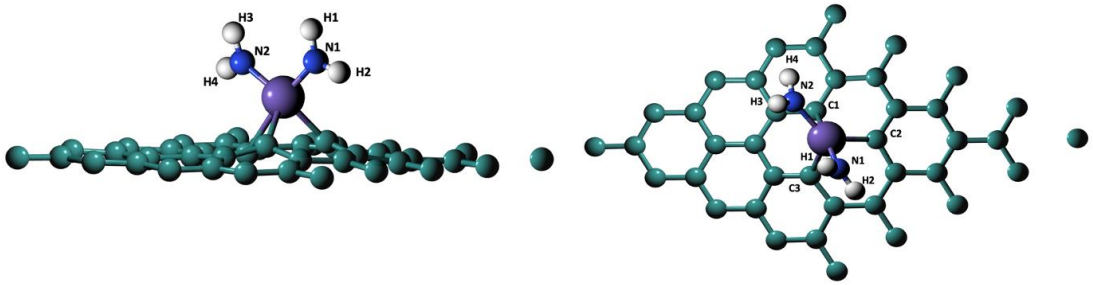

Figure 3. The adsorption of NH_2 on graphene embedded by M (M=Sc, Ti, V) a) Side view b) Top view. C atom, M metal, N atom, and H atom are illustrated by green, violet, blue and white colors respectively.

N-N bond cleavage ($N_2H_4 \rightarrow NH_2 + NH_2$) is the second reaction path on hydrazine as seen in Figure 3. The bond length of $N_1 - H_1$ and $N_1 - H_3$ squeeze on all surfaces except the $N_1 - H_3$ bond which does not change on the V metal surface as shown in Table 3 . The big differences in the bond lengths of $N_1 - H_2$ and $N_1 - H_4$ after adsorption do not occur on the surfaces but ones of $N_1 - H_2$ on V metal embedded surface shrinks from 1.021$\dot{A}$ to 1.017$\dot{A}$. The adsorption energy of NH_2 on Sc, Ti, V embedded surface are

-3.47 eV, -3.94 eV, and -4.49 eV. These adsorptions are quite stronger than that of analysis of NH_2 on pure graphene sheet (-0.778 eV) worked by Junkermeier, C.E. et al. [34]. Two NH_2 lose electrons as 1.22 e^- for Sc metal, -1.01 e^- for Ti metal and 0.87 e^- for V metal. The chemical interactions between NH_2 and graphene embedded surfaces with higher value exist compared to the adsorption on N_2H_4.

Table 3. Related parameters for NH_2 on M embedded in graphene.

	E_{ads} (eV)	d_{M-N_1} $(\dot{A})$	d_{M-N_2} $(\dot{A})$	$d_{N_1-H_1}$ $(\dot{A})$	$d_{N_1-H_2}$ $(\dot{A})$	$d_{N_2-H_3}$ $(\dot{A})$	$d_{N_2-H_4}$ $(\dot{A})$	$\Delta q(NH_2)$ (e^-)
NH_2 in the gas phase				1.025	1.021	1.025	1.021	
Sc	-3.47	2.002	2.002	1.022	1.022	1.022	1.022	-1.22
Ti	-3.94	1.918	1.926	1.021	1.022	1.023	1.02	-1.01
V	-4.49	1.89	1.90	1.023	1.017	1.025	1.022	-0.87

3.2 Hydrazine decomposition steps on graphene embedded surface

According to our knowledge, a weaker N-N bond in gaseous causes more possible the N-N bond split [21]. The below hydrazine decomposition reaction paths are used to find more proper catalysis for hydrogen production.

$$N_2H_4 \rightarrow N_2H_3 + H \quad (6)$$
$$N_2H_4 \rightarrow NH_2 + NH_2 \quad (7)$$

The configurations of the first pathway on all surfaces are viewed in Figure 4 and the configurations of the second way for all surfaces are Figure 5. The first reaction and second reaction of hydrazine decomposition are seen in Figure 6. The activation barriers (E_a) of N-H bond breakup are 1.97 eV, 1.59 eV and 0.99 respectively on Sc, Ti and V metal embedded graphene surface, while N-N bond scissions are 0.12 eV for Sc, 0.19 eV for Ti and 1.36 eV for V. The reaction energies of the N-H bond split are 1.73 eV for Sc, 0.55 eV for Ti and 0.63 eV for V, and also the reaction energy on the N-N bond scissions -1.02 eV, -1.04 eV and -1.5 for Sc, Ti and V embedded surface respectively.

The exothermic reaction gives the negative result of reaction energy while its positive result shows an endothermic reaction. An exothermic reaction occurs on the N-N bond split on all surfaces and the reactions on the N-H bond split are endothermic. Our previous finding on graphene embedded by Ni metal is that the activation barriers and the reaction energies on the N-H bond scission are respectively 0.85 eV and +0.71 eV as they are also 0.51 eV and -0.61 eV on the N-N bond scission[10].

JSR A
Journal of Scientific Reports

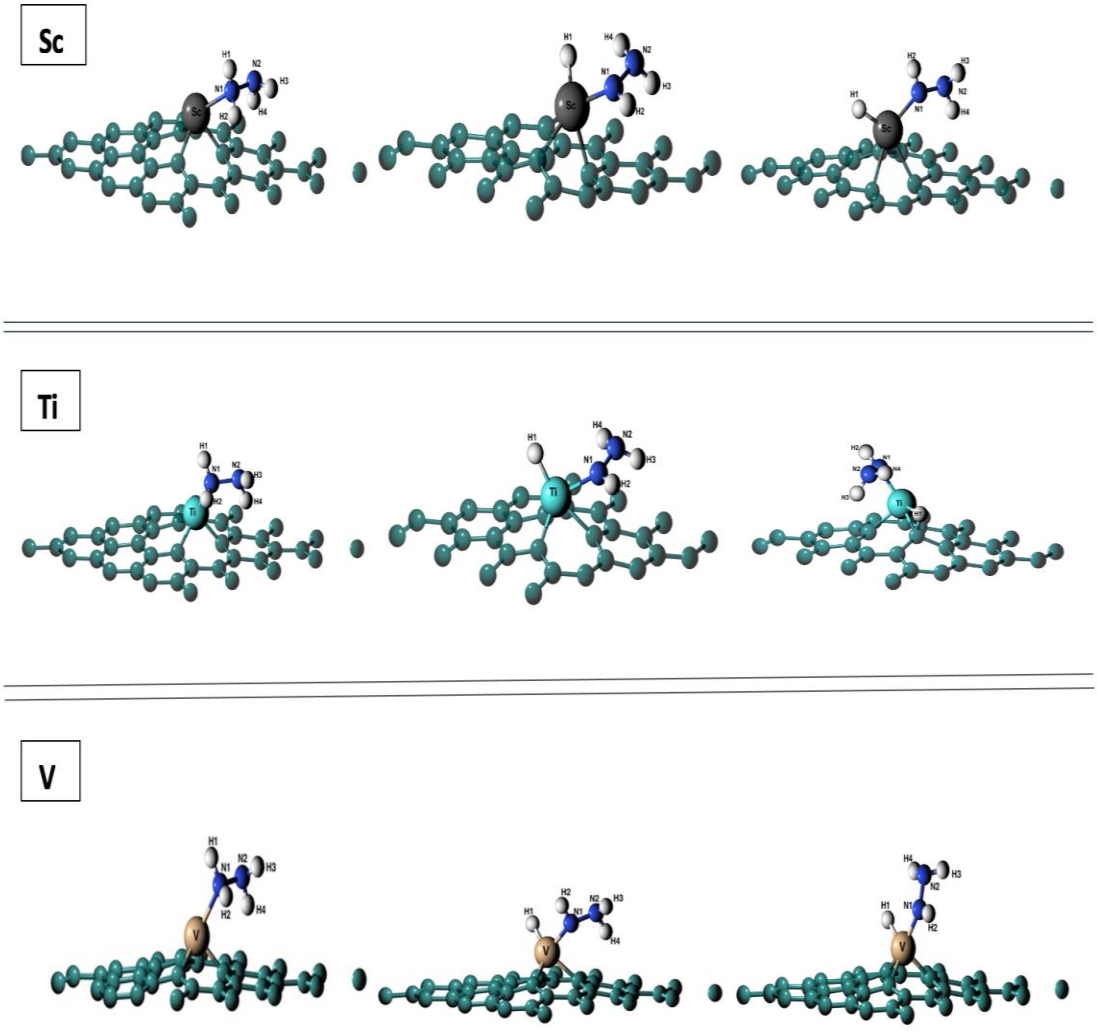

Figure 4: $N_2H_4 \rightarrow N_2H_3 + H$ pathway. The configurations of N-H bond cleavage are shown for graphene sheet various transition metal embedded surfaces. The left figure on the surface is the initial state (IS), the middle one is the conformation of the transition state (TS) and, the right figure is the final state (FS).

JSR A
Journal of Scientific Reports

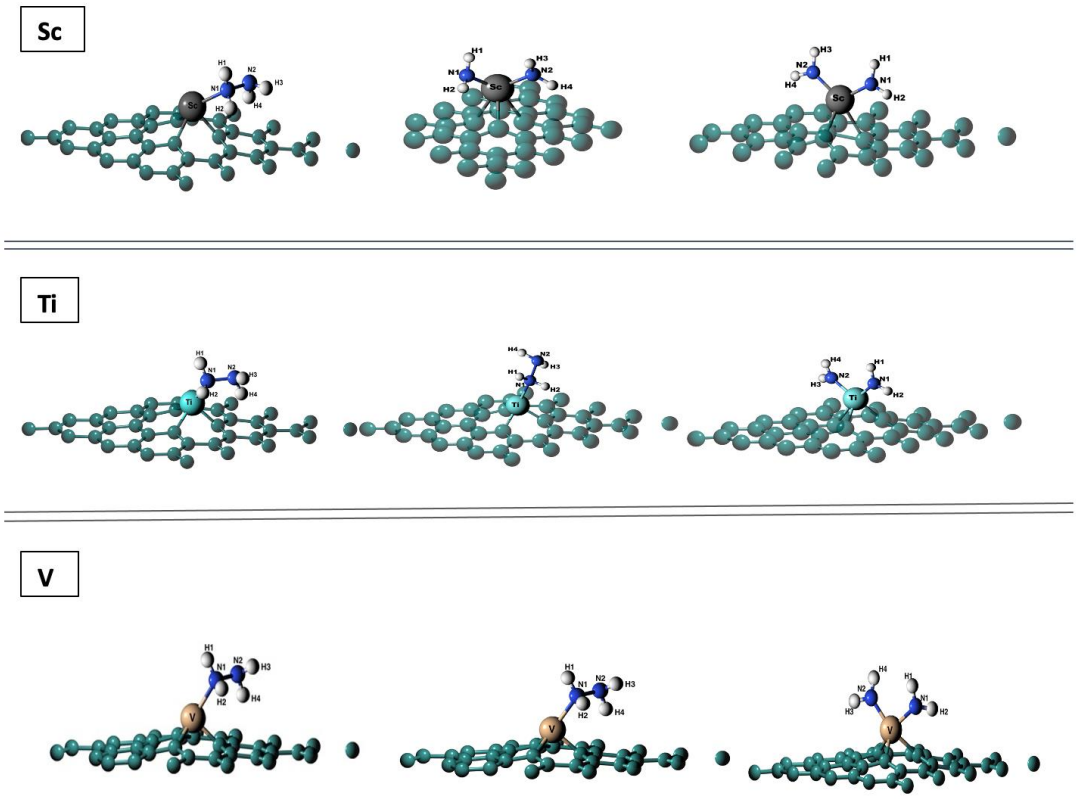

Figure 5: $N_2H_4 \rightarrow NH_2 + NH_2$ decomposition. The configurations of N-N bond cleavage are shown for graphene sheet various transition metal embedded surfaces. The left figure on the surface is the initial state (IS), the middle one is the transition state (TS) and, the right figure is the final state (FS).

JSR A
Journal of Scientific Reports

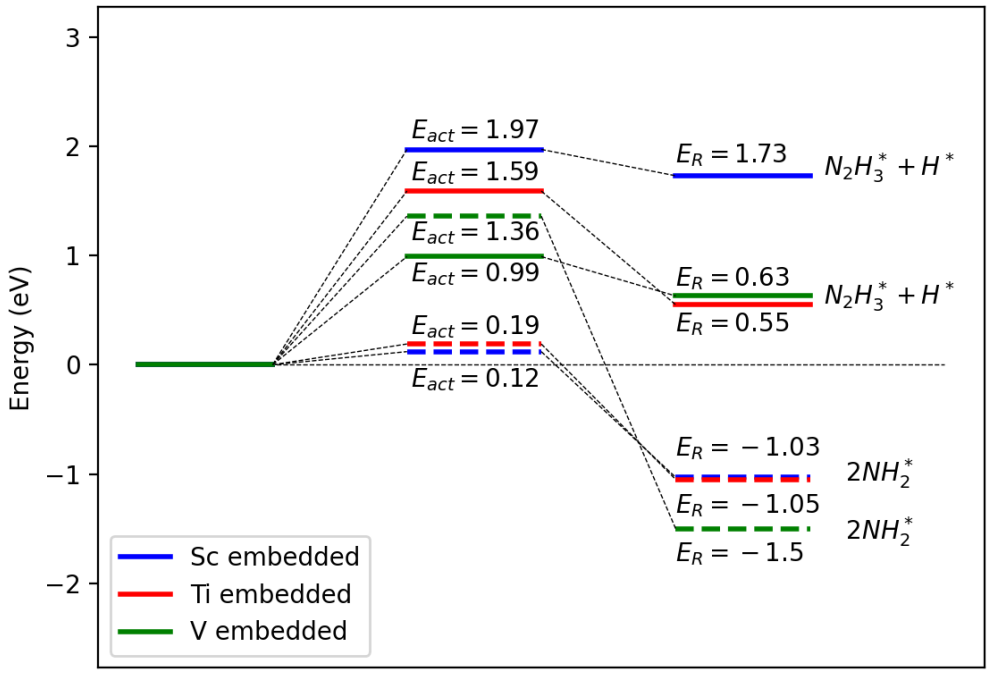

Figure 6: Hydrazine decomposition reaction energy diagram. Blue, red and green straight lines are for the N-H bond cleavages for Sc, Ti, and V respectively as their dashed lines are for the N-N bond separation.

4. CONCLUSION

In this analysis, the hydrazine decomposition reaction on Sc, Ti and V embedded graphene sheets have been investigated using hydrogen production and two NH_2 splits. The chemical interactions are observed on N_2H_4 on the surfaces so the surfaces are quite sensitive for hydrazine sensor. NH_2 splits on the Sc and Ti embedded surface can exist almost spontaneously and the main production is $2NH_2$ on these two surfaces instead of H production because they have very low activation energies. According to our result, hydrazine molecule on these two surfaces loses highly charge more than 1 e^- when it becomes $2NH_2$ compared to V metal surface, this case may cause a much weaker the N-N bond and the N-N bond splits easily. The activation energy of N-H cleavage on graphene embedded by V metal is 0.99 eV while that of N-N split is 1.36 eV. On V metal surface, H production and $2NH_2$ can be produced. NH_2 production on V metal surface does not occur immediately, first of all, the reaction must overcome an energy barrier of 0.37 eV. Therefore, this makes it more advantageous to produce H over V metal graphene. In another word, H production is more favorite than NH_2. Although previous theoretical studies found that the N-N

bond scission arises more likely than that of the N-H bond, the dehydrogenation on graphene surface embedded by V is quite promising and graphene embedded by V sheet can be efficient catalysts for hydrazine dehydrogenation.

ACKNOWLEDGEMENT

All computations calculations were made on TÜBİTAK ULAKBİM, High Performance and Grid Computing Center (TRUBA).

REFERENCES

[1] Staffell, I., et al. (2019). The role of hydrogen and fuel cells in the global energy system [10.1039/C8EE01157E]. Energy & Environmental Science, 12(2), 463-491. https://doi.org/10.1039/C8EE01157E

[2] Council, W.E. (2017). World Energy Issues Monitor.

[3] Pudukudy, M., et al. (2014). Renewable hydrogen economy in Asia – Opportunities and challenges: An overview. Renewable and Sustainable Energy Reviews, 30, 743-757. https://doi.org/https://doi.org/10.1016/j.rser.2013.11.015

[4] Peng, L. and Z. Wei. (2020). Catalyst Engineering for Electrochemical Energy Conversion from Water to Water: Water Electrolysis and the Hydrogen Fuel Cell. Engineering, 6(6), 653-679. https://doi.org/https://doi.org/10.1016/j.eng.2019.07.028

[5] Cheng, Y., X. Wu, and H. Xu. (2019). Catalytic decomposition of hydrous hydrazine for hydrogen production. Sustainable Energy & Fuels, 3(2), 343-365.

[6] Singh, S.K. and Q. Xu. (2013). Nanocatalysts for hydrogen generation from hydrazine. Catalysis Science & Technology, 3(8), 1889-1900.

[7] (2010). National Research Council (US) Committee on Acute Exposure Guideline Levels. Acute Exposure Guideline Levels for Selected Airborne Chemicals. National Academies Press (US), 8.

[8] Zheng, F., et al. (2019). Adsorption of hydrazine on XC3 (X= B, Al, N, Si, and Ge) nanosheets: A computational study. International Journal of Hydrogen Energy, 44(12), 6055-6064.

[9] Zeng, H., X. Cheng, and W. Wang. (2018). A first-principles study on adsorption behaviors of pristine and Li-decorated graphene sheets toward hydrazine molecules. Applied Surface Science, 435, 848-854.

[10] Agusta, M.K., et al. (2011). Theoretical study of hydrazine adsorption on Pt (111): Anti or cis? Surface science, 605(15-16), 1347-1353.

[11] Alberas, D.J., et al. (1992). Surface chemistry of hydrazine on Pt(111). Surface Science, 278(1), 51-61. https://doi.org/https://doi.org/10.1016/0039-6028(92)90583-R

[12] Daff, T.D., et al. (2009). Density Functional Theory Calculations of the Interaction of Hydrazine with Low-Index Copper Surfaces. The Journal of Physical Chemistry C, 113(35), 15714-15722. https://doi.org/10.1021/jp904054n

[13] Agusta, M.K. and H. Kasai. (2012). First principles investigations of hydrazine adsorption conformations on Ni(111) surface. Surface Science, 606(7), 766-771. https://doi.org/https://doi.org/10.1016/j.susc.2012.01.009

[14] Williams, J.O., et al. (1981). Ab initio studies of structural features not easily amenable to experiment: Part III. The influence of lone pair orbital interactions on molecular structure. Journal of Molecular Structure: THEOCHEM, 76(1), 11-28. https://doi.org/https://doi.org/10.1016/0166-1280(81)85109-3

[15] He, Y.B., J.F. Jia, and H.S. Wu. (2015). The interaction of hydrazine with an Rh (1 1 1) surface as a model for adsorption to rhodium nanoparticles: a dispersion-corrected DFT study. Applied Surface Science, 327, 462-469.

[16] Lu, X., et al. (2020). Mechanistic study of hydrazine decomposition on Ir (111). Physical Chemistry Chemical Physics, 22(7), 3883-3896.

[17] Yin, H., et al. (2018). Understanding of selective H2 generation from hydrazine decomposition on Ni (111) surface. The Journal of Physical Chemistry C, 122(10), 5443-5451.

[18] McKay, H.L., S.J. Jenkins, and D.J. Wales. (2011). Dissociative chemisorption of hydrazine on an Fe {211} surface. The Journal of Physical Chemistry C, 115(36), 17812-17828.

[19] Tafreshi, S.S., et al. (2014). Adsorption of hydrazine on the perfect and defective copper (111) surface: a dispersion-corrected DFT study. Surface science, 622, 1-8.

[20] He, Y.-B., J.-F. Jia, and H.-S. Wu. (2015). Selectivity of Ni-based surface alloys toward hydrazine adsorption: A DFT study with van der Waals interactions. Applied Surface Science, 339, 36-45. https://doi.org/https://doi.org/10.1016/j.apsusc.2015.02.136

[21] He, L., et al. (2017). Design strategies of highly selective nickel catalysts for H2 production via hydrous hydrazine decomposition: a review. National Science Review, 5(3), 356-364. https://doi.org/10.1093/nsr/nwx123

[22] Karaman, C., et al. (2020). Preparation of high surface area nitrogen doped graphene for the assessment of morphologic properties and nitrogen content impacts on supercapacitors. Journal of Electroanalytical Chemistry, 868, 114197. https://doi.org/https://doi.org/10.1016/j.jelechem.2020.114197

[23] Akça, A., et al. (2021). Theoretical Insights into the NH3 Decomposition Mechanism on the Cu-and Pt-Embedded Graphene Surfaces: A DFT Approach. ECS Journal of Solid State Science and Technology, 10(10), 101008.

[24] Giannozzi, P., et al. (2009). QUANTUM ESPRESSO: a modular and open-source software project for quantum simulations of materials. Journal of Physics: Condensed Matter, 21(39), 395502. https://doi.org/10.1088/0953-8984/21/39/395502

[25] Giannozzi, P., et al. (2017). Advanced capabilities for materials modelling with Quantum ESPRESSO. Journal of Physics: Condensed Matter, 29(46), 465901. https://doi.org/10.1088/1361-648x/aa8f79

[26] Kohn, W. and L.J. Sham. (1965). Self-Consistent Equations Including Exchange and Correlation Effects. Physical Review, 140(4A), A1133-A1138. https://doi.org/10.1103/PhysRev.140.A1133

[27] Blöchl, P.E. (1994). Projector augmented-wave method. Physical Review B, 50(24), 17953-17979. https://doi.org/10.1103/PhysRevB.50.17953

[28] Stefan Grimmea), J.A., Stephan Ehrlich, and Helge Krieg. (2010). A consistent and accurate ab initio parametrization of density functional dispersion correction (DFT-D) for the 94 elements H-Pu. J. Chem. Phys., 132(154104). https://doi.org/https://doi.org/10.1063/1.3382344

[29] Santos, E.J., A. Ayuela, and D. Sánchez-Portal. (2010). First-principles study of substitutional metal impurities in graphene: structural, electronic and magnetic properties. New Journal of Physics, 12(5), 053012.

[30] Mills, G. and H. Jónsson. (1994). Quantum and thermal effects in H 2 dissociative adsorption: Evaluation of free energy barriers in multidimensional quantum systems. Physical review letters, 72(7), 1124.

[31] Mills, G., H. Jónsson, and G.K. Schenter. (1995). Reversible work transition state theory: application to dissociative adsorption of hydrogen. Surface Science, 324(2-3), 305-337.

[32] Genç, A.E., et al. (2020). Hydrazine decomposition on nickel-embedded graphene. International Journal of Hydrogen Energy, 45(58), 33407-33418. https://doi.org/https://doi.org/10.1016/j.ijhydene.2020.09.035

[33] Henkelman, G., A. Arnaldsson, and H. Jónsson. (2006). A fast and robust algorithm for Bader decomposition of charge density. Computational Materials Science, 36(3), 354-360. https://doi.org/https://doi.org/10.1016/j.commatsci.2005.04.010

[34] Junkermeier, C.E., D. Solenov, and T.L. Reinecke. (2013). Adsorption of NH2 on Graphene in the Presence of Defects and Adsorbates. The Journal of Physical Chemistry C, 117(6), 2793-2798. https://doi.org/10.1021/jp309419x